Research Article

Alyaa Abdulrazzaq Azeez*, Azhar Ayad Jaafar, Mustafasanie M. Yussof and Abrahem A. Ali Blash

Study of the behavior of reactive powder concrete RC deep beams by strengthening shear using near-surface mounted CFRP bars

https://doi.org/10.1515/eng-2022-0433
received January 06, 2023; accepted March 21, 2023

Abstract: The applications of modern materials especially reactive powder concrete for improving concrete structures have been significantly growing in recent years. Great conduct properties creep, shrinkage, little permeability, ultra-high strength, and expanded safety against corrosion are the important features of Reactive Powder Concrete. In addition, the use of the Near-Surface Mounted technique in recent decades has helped strengthen and repair shears-reinforced concrete (RC) for deep beams using carbon fiber replacement reinforcing bars. The parameters studied in the present research investigated the impact of the maximum load, deflection, stress–strain curve of concrete, first shear crack, crack pattern, and crack width. Considering the aforesaid cause and objective, one specimen of Reactive Powder Concrete RC deep beams has a rectangular cross-section of 150 mm in width, 500 mm in depth, and a total length of 1.2 m. One control specimen was tested for comparison. In addition, 12 control specimens (cylinder and cubes) are used for experimental investigation on the mechanical properties of normal and Reactive Powder Concrete deep beams. Following the specimens' processing, they were subjected to one concentrated load pressure test through a hydraulic jack. Moreover, six core drill specimens were taken from those deep beams to obtain the real mechanical properties of those beams, including maximum stress, modulus of elasticity, density, stress–strain curve, and Poisson's ratio, after subjecting them to the pressure machine. Depending on the results, the ultimate strength, deflection, and first shear crack capacity for the specimens (RPCDB1P-4NSM & RPCDB1P-8NSM) have increased by (21, 25), (47, 27), and (133, 150)%, respectively, compared with (CDB1PC20). Moreover, the specimens above have reduced the first shear crack width by (9, 33.25)% respectively compared with (CDB1PC20) at 65% of the ultimate shear load.

Keywords: deep beams, RPC, NSM, CFRP bars, stress–strain curve, maximum load

Nomenclature

RPC	Reactive Powder Concrete
RPCDB	Reactive Powder Concrete Deep Beam
NSM	Near-Surface Mounted
RC	Reinforced concrete
FRP	Fiber-Reinforced-Polymer
CFRP	Carbon Fiber Reinforcement Polymer
CDB	Control Deep Beam
CDB1PC20	Control Deep Beam one-point load compressive strength concrete (20 MPa)
RPCDB1P-4NSM	Reactive Powder Concrete Deep Beam one point load 4CFRP bars (NSM)
RPCDB1P-8NSM	Reactive Powder Concrete Deep Beam one point load 8CFRP bars (NSM)
ffu	ultimate tensile strength of concrete
f'_c	cylindrical compressive strength of concrete
f'cu	cubic compressive strength of concrete
f'_{dc}	drilling core compressive strength conc.
Ec	modulus of elasticity of concrete

1 Introduction

Shear is one of the most dangerous types of failure in reinforced concrete (RC) structures because it happens

* Corresponding author: Alyaa Abdulrazzaq Azeez, Ministry of Education, Najaf, Iraq, e-mail: alyaaabdulrazzaq@yahoo.com
Azhar Ayad Jaafar: School of Civil Engineering, Engineering Campus, Universiti Sains Malaysia, Nibong Tebal 14300, Pulau Pinang, Malaysia; Ministry of Education, Najaf, Iraq, e-mail: Azhr1983@student.usm.my
Mustafasanie M. Yussof: School of Civil Engineering, Engineering Campus, Universiti Sains Malaysia, Nibong Tebal 14300, Pulau Pinang, Malaysia, e-mail: cemustafa@usm.my
Abrahem A. Ali Blash: School of Civil Engineering, Engineering Campus, Universiti Sains Malaysia, Nibong Tebal 14300, Pulau Pinang, Malaysia; College of Engineering Technology - Houn, Houn, Libya, e-mail: blash1985@gmail.com

suddenly and without warning, like the shear failure that occurs in deep beams. Recent studies have found that current RC beams suffer from shortcomings in shear and require strengthening. Deficiencies can occur due to several factors such as insufficient shear reinforcement resulting from design or construction errors or use of outdated codes, reduction in the steel area due to corrosion, and increase in demand for service load (Khalifa *et al.*) [1].

The use of FRP materials has been rapidly expanding throughout the world in order to achieve the modern reinforcement and repair of existing concrete structures (Katsumata et al., Grace and Sayed, Rostasy et al., Al-Mahmoud et al.) [2–5]. An effective technique for Fiber Reinforced Polymer (FRP) with Near Surface Mounted (NSM) technology has been used to improve the bending and shear behavior of existing or newly reinforced structural elements (Hatem *et al.*) [6]. A widely accepted solution is the use of fiber-reinforced polymers (FRP) to strengthen RC structural elements in bending and shearing areas due to this technology's advantages over other traditional strengthening methods (Saadah *et al.*) [7]. Moreover, the use of high-performance concrete, such as reactive powder concrete (RPC), has been observed, which has high-performance properties that will limit the failure of shear to contain a few steel fibers in its mixture.

Strengthening techniques using fiber-reinforced-polymer (FRP) laminates have been developed since the 1980s. FRP materials present better mechanical, physical, and chemical properties than steel ones. The applications of FRP materials for retrofitting and strengthening existing concrete structures have grown rapidly around the world (Meier, Steiner, Nanni, Matthys et al., Blasi et al., Labossière et al., Hazen et al., Ichimasu et al., Katsumata et al., AL-Mahmoud et al., Rostasy et al. (2004), Grace and Sayed Abdel (2003)) [8–17].

In addition, with the advent of a new technique such as NSM, which will require investigation into its potential applications, for example, the use of NSM CFRP bars with other types of concrete such as ultra-high performance concrete RPC as a strengthening or repair of the shear for deep beams. Also, until recently, no researchers have conducted the strengthening or repairing of RPC deep beams using NSM CFRP rods.

Today, it is considered good to adopt the use of promising modern materials and technologies and compare their performance with the maintenance methods used in the past, medium to a long period. This will help close the research gap for applying the NSM technique in controlling bending and shear failure in the long term.

2 Experimental program

The testing matrix contained two simply supported RC deep beam specimens with and without reactive powder concrete (RPC), with a total span (*L*) of 1,200 mm, overall depth (*H*) of 500 mm, width of 150 mm, and shear span to effective depth ratio (a/d) equal to 0.77. All beams were tested under a three-point loading configuration as shown in Figure 1. Three Ø16-mm deformed bars were provided as longitudinal tension reinforcement for the bottom zone, two Ø12-mm as longitudinal tension reinforcement for the top zone, and Ø12-mm @200 mm c/c for stirrups. The concrete cover was 40 mm.

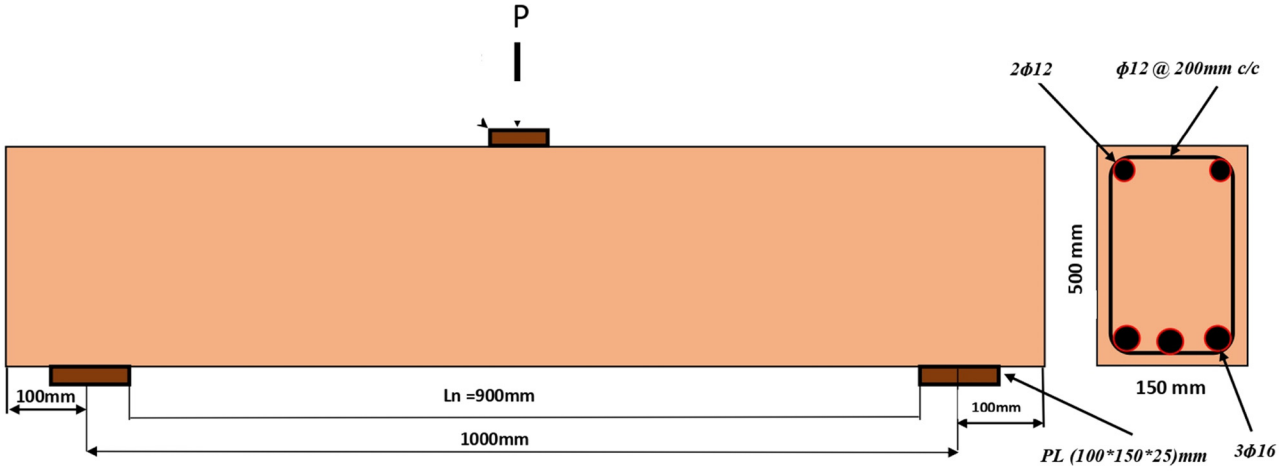

Figure 1: Specifications of tested reinforced concrete deep beams with and without RPC.

2.1 Material properties

The specifications of materials used in this research and their suitability for making the RPC are explained here.

2.1.1 Cement

The type of cement is ordinary Portland cement of the KAR Group factory in Al-Najaf. It conforms to Iraqi Standard Specification I.Q.S. No. 5 (IQS) [18]. The physical and chemical tests of the cement were conducted at Kufa University and the laboratories of the engineering consulting bureau.

2.1.2 Fine aggregate

Natural sand locally available from the Al-Najaf region was used for concrete mixes in this research. In reactive powder concrete, all large size of particles must be eliminated, and very fine sand aggregate is used in order to produce a very dense form. The fine aggregate was passed from sieve No. 40 (450 μm) maximum size and remained on sieve No. 100 (150 μm) (single grading) (Richard and Cheyrezy) [19]. The chemical and physical tests of fine aggregate were conducted at Kufa University and laboratories of the engineering consulting bureau.

2.1.3 Silica fume

Silica fume is a highly reactive material that can be used in comparatively small quantities to improve the characteristics of concrete ACI 234R (ACI) [20]. Also, silica fume is described as "very fine non-crystalline silica produced in electric arc furnaces for silicon or alloys containing silicon." It is usually a gray-colored powder, slightly like Portland cement or some fly ashes. One of the most substantial components of reactive powder concrete is using pozzolanic material. It is not only used to give extra binders but also used as a filler. The present manuscript has used densified silica fume (Sika® Fume S 92 D). The micro silica used in this research was based on the physical and chemical limitations of ASTM C1240 (ASTM) [21].

2.1.4 Superplasticizer

GLENIUM® 54 is a third-generation superplasticizer for concrete and mortar. It achieves the limitations for superplasticizers regarding ASTM C494/C494M (ASTM) [22]: types A and F. It was used as a water-reducing admixture with a nominal dosage of 2% of cement weight. This mixture gives high water shorthand (causing high strength and density), excellent workability without bleeding or segregation, and very high early and high ultimate strength concrete with minimal voids and therefore optimum density and improved water impermeability and surface finish.

2.1.5 Steel fibers

RPC contains small steel fibers instead of coarse aggregates. Steel fibers are used in reactive powder concrete to enhance some properties and improve ductility. The steel fiber has a length of almost (13 mm) and a diameter of about (0.2 mm) based on ASTM A820/A820M (ASTM) [23]. The steel fibers used in this research were straight steel fibers manufactured by the Bekaert Corporation with a volumetric ratio of 0.7%. The properties of steel fibers obtained from China are given in Table 1.

2.1.6 Steel reinforcing bars

Shear design is a very required factor when starting the design of a deep beam, especially the ACI code 11.8. A deep beam has a clear span of a depth ratio of less than five for divided overloading requirements [24]. Reinforcing steel used as longitudinal bars and web reinforcement in RC deep beams met the ASTM A615, 1990 [25]. Two sizes of bars (Ø 16 mm and Ø12) were used as longitudinal and stirrup reinforcement to reinforce all deep beams tested the specimen of the Ukrainian reinforcement steel bars was tested in tension and shear to determine its mechanical properties. The results are shown in Table 2. The tensile tests of the specimens were executed by the testing machine available at Kufa University and laboratories of the engineering consulting bureau.

Table 1: Properties of steel fibers*

Property	Value
Length	13 mm
Diameter	0.2 mm
Density	7,800 kg/m^3
Tensile strength	2,600 MPa
Aspect ratio	65

*Supplied by the manufacturer.

Table 2: Characteristics of steel reinforcement

Property	Value Ø16	Value Ø12
Nominal diameter (mm)	16	12
Area (mm^2)	201	113
Yield stress (MPa)	580	338
Ultimate strength (MPa)	710	498
Elongation at ultimate strength (%)	13.25	14.35

3 Specimens' preparation

For this study, 20 mm thick four-plywood formworks were used to cast three beams in each casting process. Next, all formworks were coated with formwork oil at the inner surface of the formwork so that the detaching process of the beam afterward would be easier. A mixer was used to mix the concrete. The rebar cages were placed inside the forms and held in place by a 2.5 cm plastic chair to ensure that the proper cover was maintained. Before mixing, all the quantities were weighed by a sensitive electronic to ensure accurate measurement of quantities and packed in a clean metals container prior to starting the rotation of the mixer materials. First, the mixer was operated, and then, the fine aggregate, cement, silica fume, and water were added while the mixing was running some of the mixing water and Superplasticizer were added. finally, the fiber steels were added to all mixed concrete. The concrete mix time was about 30 s after all ingredients were put in the mixer. Twelve cylinders (100 × 200) for each series were cast to specify the concrete properties. The concrete was then poured into six layers to make sure the compaction process was sufficient and not overly done. Insufficient compaction could cause incompact concrete and the form of a honeycomb in the specimens. All things mentioned above are shown in Figure 2.

4 Concrete mix design

Before starting the concrete mix, a slump test was taken for the concrete mix. Many trial mixes were originally used in this scientific article before reaching the required performance of the RPC. The dominant mix proportioning (by weight) for all beams and their reference specimens (cubes, cylinders, and drilling cores) was 1:1:0.08 (cement: fine sand: silica fume) with a water-to-cement ratio of 0.25. The superplasticizer was used with a proportion of 2% by the cement weight, and steel fiber with a volume fraction of 0.7% was used in all mixes (Table 3).

The following specimens were cast to specify the properties of the hardened concrete:

- 100-mm-diameter × 200-mm-long cylinders based on ASTM C39 [26] for compressive strength and based on ASTM C496 [27] (the split-cylinder test) for tensile strength.
- 150-mm × 150-mm cubes based on ASTM C39 [26]. for compressive strength.
- 150-mm-diameter × 150-mm-long drilling core specimens for getting real mechanical properties based on ASTM C42/C42M-18a [28]. such as (compressive Strength, Modulus of elasticity, poison's ratio, stress-strain curve, and longitudinal-lateral strain).

5 Strengthening procedure

The preparation of the strengthened beams involves cutting the grooves on the sides of the beams, and application of the NSM CFRP rods. After the beams had been cured properly, the concrete was cut using a special machine to make grooves, and all the grooves had square cross-sections, with a depth and width of 10 mm as shown in Figure 3. Then, the grooves were cleaned with jet water to remove the concrete powder produced during the cutting process as shown in Figure 4. After that, the epoxy paste was prepared by mixing resin and hardener in 2:1 proportion by volume with a power mixer as shown in Figure 5. The groove was filled halfway with the paste. Next stage, the rod was then placed in the groove and pressed lightly. The groove was then filled with more paste to the surface level as shown in Figure 6. The specimens remained in the laboratory environment for two weeks before being tested. After completing the CFRP rods installation within two days, all apparent concrete surface specimens were painted white to easily detect the crack patterns (growth of crack) before testing as shown in Figure 7.

6 Testing procedure

After the beams were removed from the water at the age of 28 days. Also, the beam specimens were cleaned and painted in order to show crack diffusion. All beam specimens were tested under a static one-point load test to study their behavior by a universal testing machine as shown in Figure 8. The test was stopped at every 10 kN to register the evolution of cracks, strains, and deflections along the beam, and the specimens were positioned in the universal testing machine for midpoint loading. The deflection dial

Figure 2: Specimens' preparation and materials of RPC.

Table 3: Mechanical properties of deep beam specimens

Beam	f'_c (MPa)	f'_{cu} (MPa)	f'_{dc} (MPa)	ffu (MPa)	Ec (Exp.)* (GPa)	Ec (Equation (1)) (GPa)*	Ec (Equation (2)) (GPa)*	υ*
CDB*	32.7	38.7	25	2.20	23.5	26.8	25.88	0.2
RPCDB*	61.8	66.3	55.2	2.80	42.5	—	—	0.25

*Ec(Exp.) modulus of elasticity of concrete based on (ASTM C469-02) [29] and which it calculates from stress-strain curve by slop = Rise/Run.
*Ec(Equation (1)) modulus of elasticity of ordinary concrete based on (ACI-318M-14) [30] and which it computes by equation (1), $EC = 4{,}700\sqrt{\text{fc}'}$.
*Ec(Equation (2)) modulus of elasticity of ordinary concrete based on (ACI 363R-92) [31] and which it computes by equation (2), $EC = 3{,}320\sqrt{fc'} + 6{,}900$.
υ Poisson's ratio based on (ASTM C469-02) [29]. CDB – Concrete deep beam. RPCDB* – Reactive powder concrete deep beam.
Note: (1) The values of (f'_c, f'_{cu}, f'_{dc}, and ffu) were calculated for an average of three specimens. (2) We can note that the above two equations are for calculating (Ec) for ordinary concrete only, and there is no equation for calculating (Ec) for reactive powder concrete until now (3). We can observe that the value of the drilling core compressive (f'_{dc}) is a real and very different value compared with the two values of f'_c, f'_{cu}. For the CDB specimen, where f'_{dc} differs with (f'_c, f'_{cu}) by (30, 55%), respectively. For the RPCDB specimen, where f'_{dc} differs with (f'_c, f'_{cu}) by (12%, 20%), respectively.

Figure 3: Making grooves.

Figure 4: Grooves cleaning.

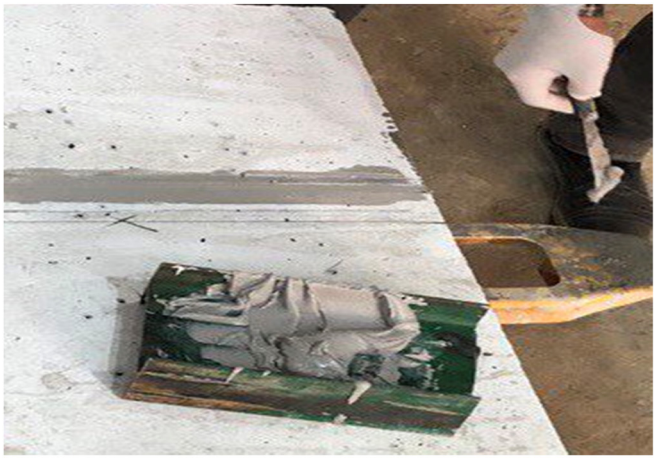

Figure 5: Mixing of epoxy paste.

Figure 6: Specimen filling with epoxy paste.

Figure 7: Specimen painting.

gauge was placed at its marked position to touch the bottom face of the beam center. When the beam showed deterioration with increasing deformation, the ultimate load was registered, and the load was removed to take

Figure 8: Universal testing machine and sample under one-point load.

Figure 9: Taking drilling core samples.

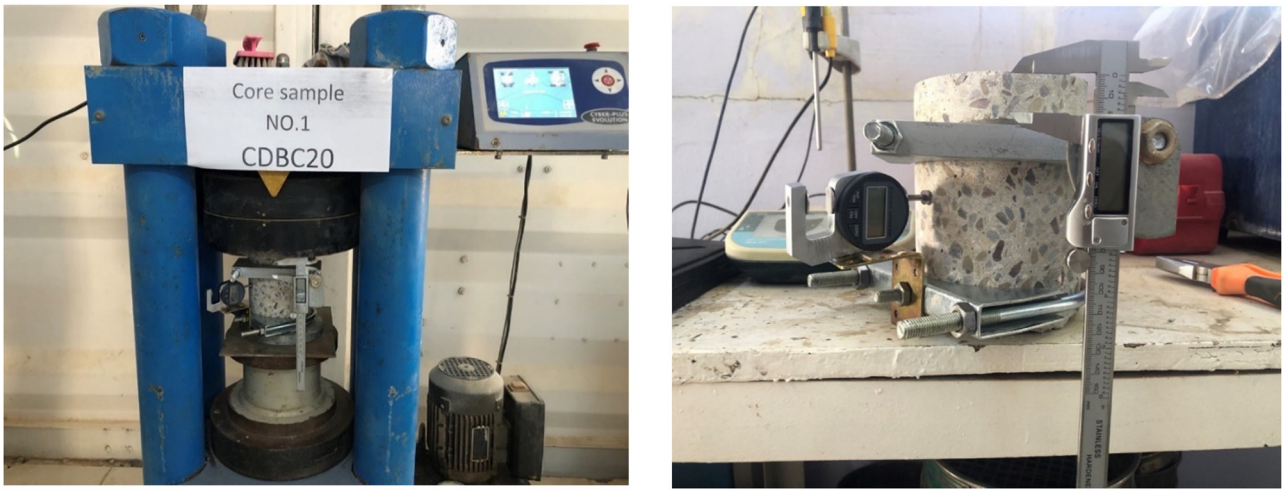

Figure 10: Testing compression machine with two gauges to calculate the strains.

photographs of the final crack pattern. In addition, after the failure, (6) core drill specimens were taken from undamaged areas of deep beams as shown in Figure 9, which will be divided into three specimens from the deep beam with ordinary concrete and three specimens from the deep beam with reactive powder concrete, which will be

subjected to examination by the compression machine using a digital caliper and mini digital thickness gauge which have been manufactured manually and using them with the compression machine as shown in Figure 10 to get the real mechanical properties especially stress–strain curve.

7 Results and discussion

The obtained experimental results are summarized in Table 4, including the first cracking load, ultimate load, ultimate shear strength, and crack patterns-failure mode. In addition, comparisons of load–deflection behavior, shear crack width, and stress–strain curve of these beams are shown in Figures 11–18. The specimen control deep beam one-point load compressive strength with 20 MPa (CDB1PC20) failed to shear. The first flexural crack was visible at approximately 16% of the 80 kN load, followed by another crack at the 120 kN load. With increasing load, the flexural cracks spread more but stopped at 280 kN loading. On the other hand, the first shear crack was observed at 120 kN loading from the inner edge of the support. When the load increased to 260 kN, another primary shear crack appeared in the center of the support. By increasing the load, bending and shear cracks spread and mature. Upon reaching the failure load, the main diagonal slit occurred at an angle of 53° as shown in Figure 19. The specimen CDB1PC20 failed when the load reaches 480 kN or the shear load is 240 kN.

From observation, the beam suddenly failed, and the failure mode was due to the failure of the shear pressure. The specimen reactive powder concrete deep beam one-point load using four CFRP bars (RPCDB1P-4NSM) failed in the flexural region and did not fail to shear due to the use of the near-surface mounted strengthening technique. The first flexural crack appeared in the middle of the beam when the load was about 100 kN. Other small cracks appeared widely between the two supports starting from below toward the bearing points as the load gradually began to increase. Other oblique shear cracks (in both shear periods on the left and right sides of the beam) initially formed at different points at a load of 280 kN and spread towards the loading points. With overloading, these cracks quickly spread and widened. The beam failed to flexural, and the failure occurred in the middle of the beam, as shown in Figure 20. RPCDB1P-4NSM failed at loading up to 580 kN or a shear load of 290 kN. From observation, the packet failed after a period of loading and the failure mode was due to the failure of the flexural compression. Also, from the significant decrease in the shear capacity of the CDB compared to that of the RPCDB1P-

Table 4: Mechanical properties of deep beam specimens

Beam	First shear crack capacity (kN)	Ultimate capacity (kN)	Shear force (kN)	Increase in the first shear crack capacity (%)	Increase in ultimate capacity (%)	Modes of failure
CDB1PC20	120	480	220	0 (Reference)	0 (Reference)	Shear – Compression
RPCDB1P-4NSM	280	580	290	1.33	21	Flexural – Compression
RPCDB1P-4NSM	300	600	300	1.5	25	Flexural – Compression

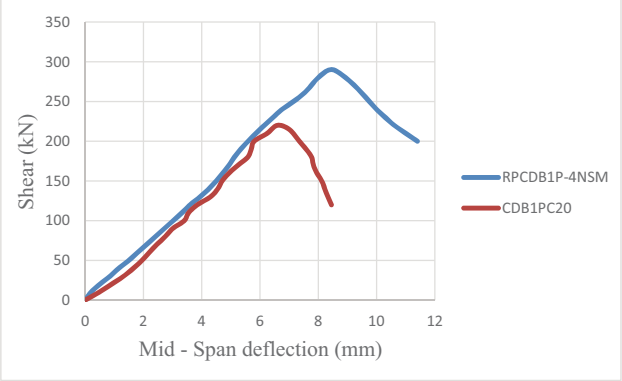

Figure 11: Deflection profile for beams in CDB1PC20and RPCDB1P-4NSM.

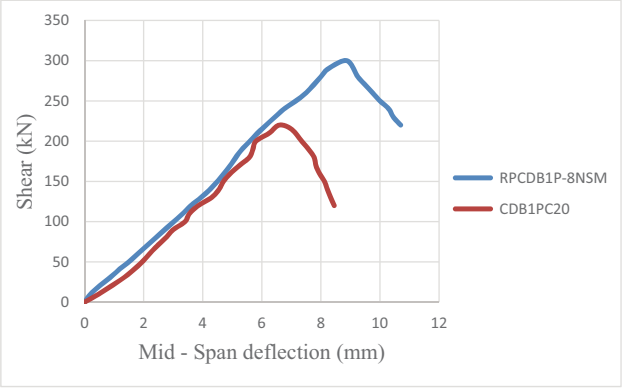

Figure 12: Deflection profile for beams in CDB1PC20 and RPCDB1P-8NSM.

4NSM beam, the presence of the polymer rods used with the specimen with reactive concrete powder reduces the shear ability. The shear capacity of the RPCDB specimen decreased by 20% compared to the shear capacity of the CDB specimen.

For the specimen reactive powder concrete deep beam one-point load using four CFRP bars (RPCDB1P-8NSM) failed in the flexural region and did not fail to shear due to the use of the Near-Surface Mounted strengthening technique. The first flexural crack appeared in the middle of the beam when the load was about 100 kN. Other small flexural cracks appeared for a period of loads ranging (180–260) kN. When the load began to gradually increase, shear cracks were formed, but they remained at a short length at the abutment and did not extend to the loading points due to the strengthening NSMCFRP rods technique close to the surface, where the first shear crack was formed at the load of 300 kN and stopped until the gestation period of 340 kN and equally from both sides of the threshold at the supports. The beam failed in flexural, and the failure occurred in the middle of the beam, as shown in Figure 21.

$$\% \text{ Increase } = \frac{P(\text{Strengthened}) - P(\text{Reference})}{P(\text{Reference})}$$

The deflection profile for beams CDB1PC20 and RPCDB1P-4NSM is clearly shown in Figure 11. The deflection was recorded at every load increment until failure. Based on the observation, a deflection value of 9.73 mm was recorded for beam RPCDB1P-4NSM at the highest peak but only 6.59 mm for beam CDB1PC20. However, beyond the failure load, the post-peak behavior for RPCDB1P-4NSM and CDB1PC20 showed similar trends, that is, a reduction in load but with a gradual increase in deflection. The post-peak increment in deflection was more gradual for beam RPCDB1P-4NSM compared to CDB1PC20. Prior to total failure, a maximum deflection of 11.40 mm for RPCDB1P-4NSM and 8.45 mm for CDB1PC20 was recorded.

In addition, the deflection profile for beams CDB1PC20 and RPCDB1P-8NSM is clearly shown in Figure 11. The

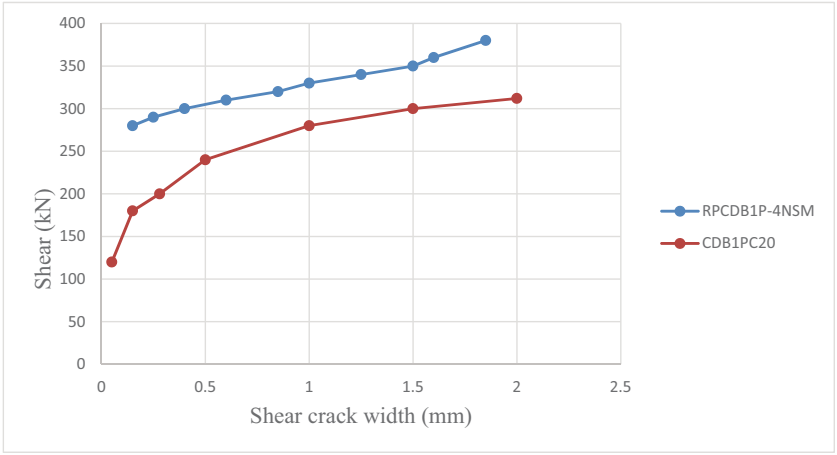

Figure 13: Crack width profile for beams in CDB1PC20 and RPCDB1P-4NSM.

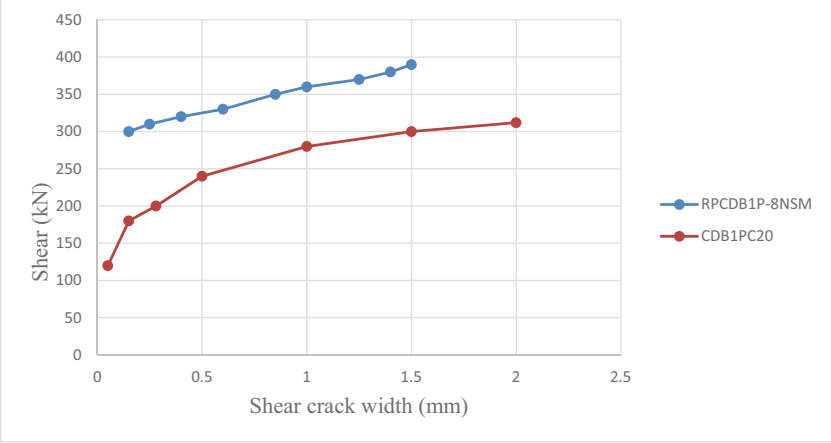

Figure 14: Crack width profile for beams in CDB1PC20 and RPCDB1P-8NSM.

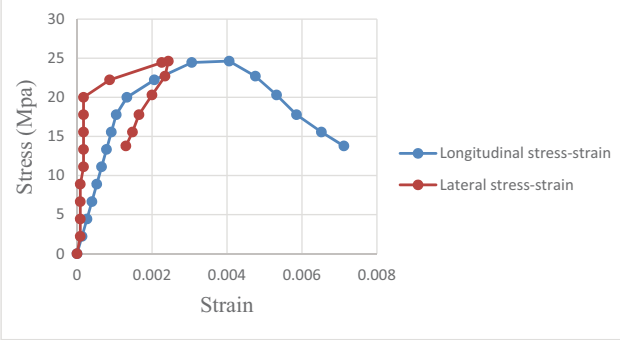

Figure 15: Stress–strain for beam CDB1PC20.

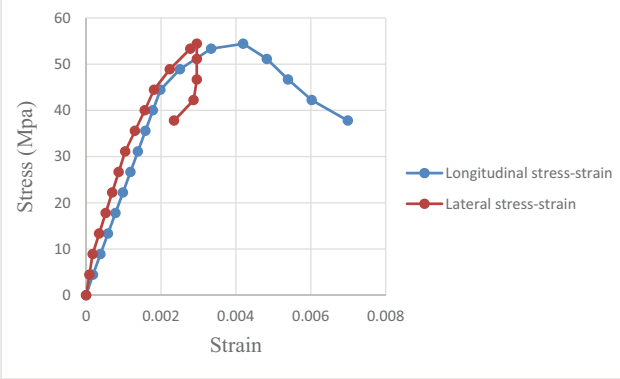

Figure 16: Stress–strain for beam RPCDB1P-4NSM.

deflection was recorded at every load increment until failure. Based on the observation, a deflection value of 8.40 mm was recorded for beam RPCDB1P-8NSM at the highest peak but only 6.59 mm for beam CDB1PC20. However, after the failure load, the subsequent peak behavior of (RPCDB1P-8NSM) and (CDB1PC20) showed similar trends,

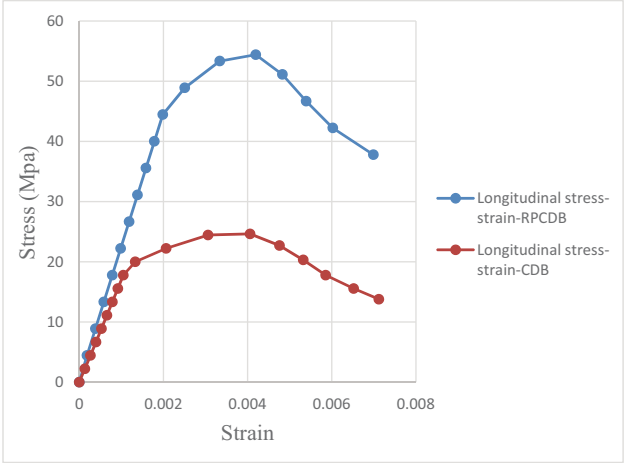

Figure 17: Stress–strain for beam RPCDB1P-4NSM and CDB1PC20.

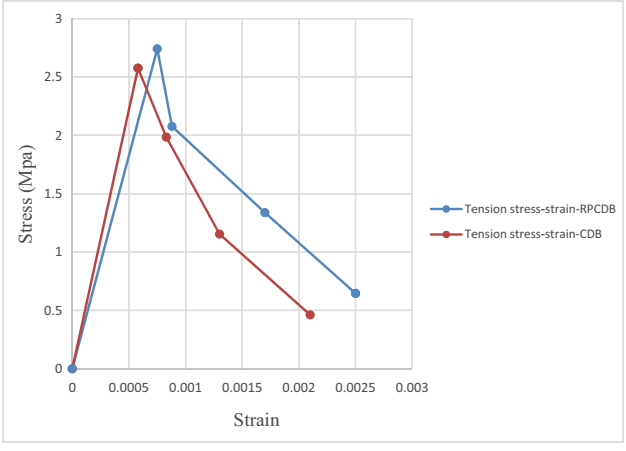

Figure 18: Stress–strain curve for tension zone in beams RPCDB1P-4NSM and CDB1PC20.

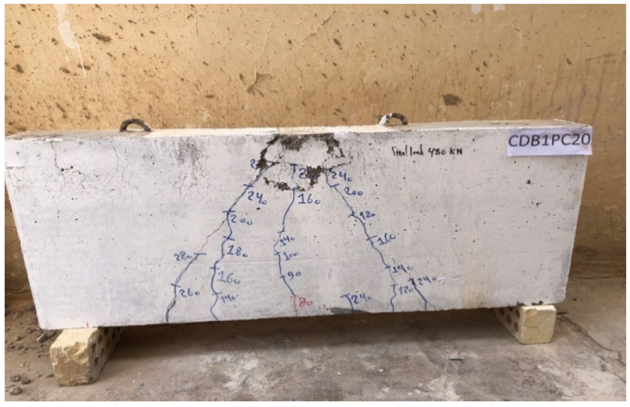

Figure 19: Crack pattern and failure mode CDB1PC20.

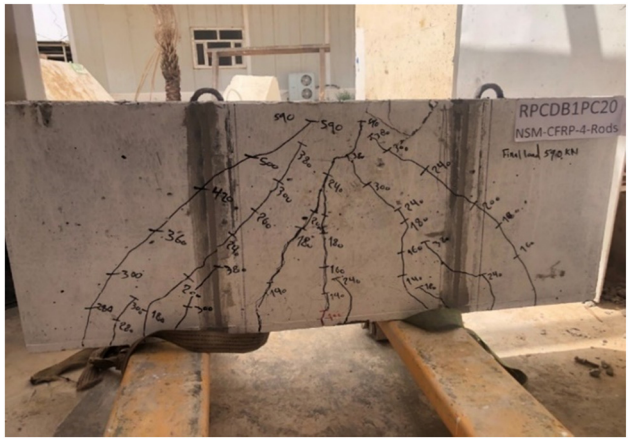

Figure 20: Crack pattern and failure mode RPCDB1P-4NSM.

that is, a decrease in load but with a gradual increase in deviation. The post-peak increment in deflection was more gradual for beam RPCDB1P-8NSM compared to CDB1PC20. Prior to total failure, a maximum deflection of 10.70 mm for RPCDB1P-4NSM and 8.45 mm for CDB1PC20 was recorded.

On the other hand, shear crack width was measured and recorded during every load increment. For control beam CDB1PC20, the first shear crack appeared at 120 kN, and the crack width value was measured at 0.05 mm. The crack width continued to increase with every load increment, and at 65% of the ultimate shear load (312 kN), the value for the diagonal crack had increased to 2 mm. Moreover, the first shear crack of the RPCDB1P-4NSM beam occurred at a load of 280 kN, and the crack width value was measured at 0.15 mm as a load was increased; the shear diagonal crack at 1.8 mm was recorded at the load of 377 kN. Figure 13 shows the shear crack width development for specimens CDB1PC20 and RPCDB1P-4NSM loading.

In addition, shear crack width was measured and recorded during every load increment. For control beam CDB1PC20, the first shear crack appeared at 120 kN, and the crack width value was measured at 0.05 mm. The crack width continued to increase with every load increment, and at 65% of the ultimate shear load (312 kN), the value for the diagonal crack had increased to 2 mm. Moreover, the first shear crack of the RPCDB1P-8NSM beam occurred at a load of 300 kN, and the crack width value was measured at 0.15 mm; as the load was increased, the shear diagonal crack at 1.5 mm was recorded at a load of 390 kN. Figure 14 shows the shear crack width development for specimens CDB1PC20 and RPCDB1P-8NSM loading.

From observation, the beam (RPCDB1P-4NSM) delayed the appearance of the first shear crack by (133%) with respect to the load compared with the beam (CDB1PC20) due to the higher shear capacity of the specimen (RPCDB1P-4NSM). Moreover, the beam (RPCDB1P-4NSM) reduced the first shear

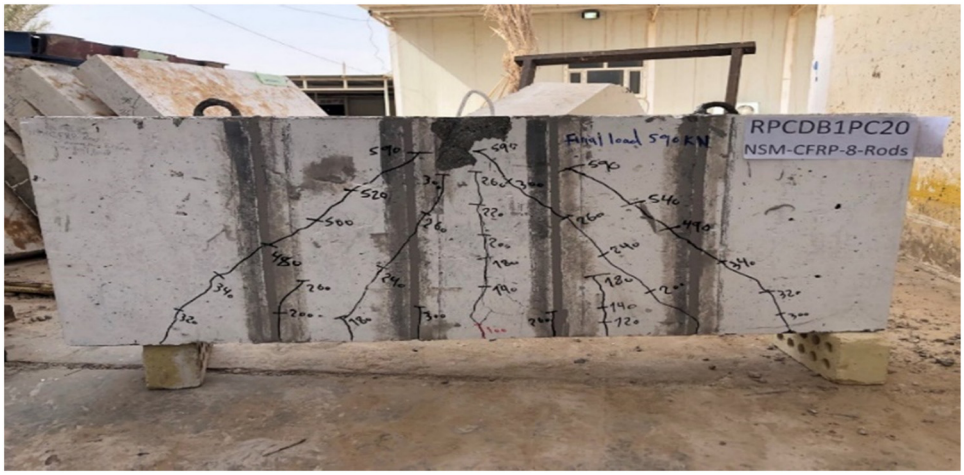

Figure 21: Crack pattern and failure mode RPCDB1P-8NSM.

crack width by (9%) compared with the beam (CDB1PC20) at (65%) of the ultimate shear load.

In addition, the beam (RPCDB1P-8NSM) delayed the appearance of the first shear crack by (150%) with respect to the load compared with the beam (CDB1PC20) due to the higher shear capacity of the specimen (RPCDB1P-8NSM). Moreover, the beam (RPCDB1P-8NSM) reduced the first shear crack width by (33.25%) compared with the beam (CDB1PC20) at (65%) of the ultimate shear load.

From the drilled core test based on ASTM C42/C42M-18a [28] applied on beams (RPCDB1P-4NSM) and (CDB1PC20), real and realistic data for those deep beams were obtained, which were translated in the form of stress-strain curves which including longitudinal and lateral stress–strain curve for concrete compression zone of beams (CDB1PC20) and (RPCDB1P-4NSM) as shown in Figures 15 and 16. The longitudinal stress–strain curve for the concrete compression zone for (CDB1PC20) and (RPCDB1P-4NSM) specimens was combined with one aggregation curve to compare the results between these two specimens as shown in Figure 17.

In Figure 17, the stress–strain curve of the control specimen is shown in the (CDB1PC20) specimen, the shape of the sample is evident, and the drop is also seen at the end of the loading. However, the behavior of the (RPCDB1P-4NSM) specimen is very different compared to that of the (CDB1PC20) specimen of the higher stress and decreased strain of the reactive powder concrete deep beam, and this is evident by the high peak and little extension of the curve.

Young's modulus increased from 27,932 MPa for reference mixings to 43,029 MPa for mixings that have 10% silica fume powder. In addition, the flexural strength rises by rising silica fume to 12.5%; then, after this value decrease [26].

From the split-cylinder test based on ASTM C496 [27], the stress–strain results were obtained for the concrete tensile zone for CDB1PC20 and RPCDB1P-4NSM specimens as shown in Figure 18. In Figure 18, the stress–strain curves for the stress in the tension zone for CDB1PC20 and RPCDB1P-4NSM specimens; it can be observed that the tension stress of beam RPCDB1P-4NSM is higher than beam CDB1PC20. Moreover, the strain of specimen beam RPCDB1P-4NSM is higher than that of specimen CDB1PC20. The increase in tensile stress for the RPCDB1P-4NSM specimen at maximum stress compared with the CDB1PC20 specimen is 10%, while the increase in tensile strain for the RPCDB1P-4NSM sample at maximum stress is 29%.

All the stress–strain results for specimens RPCDB and CDB were compared based on the results of previous studies as shown in Figure 22. It showed an acceptable agreement with those results, which proves the validity of these laboratory results.

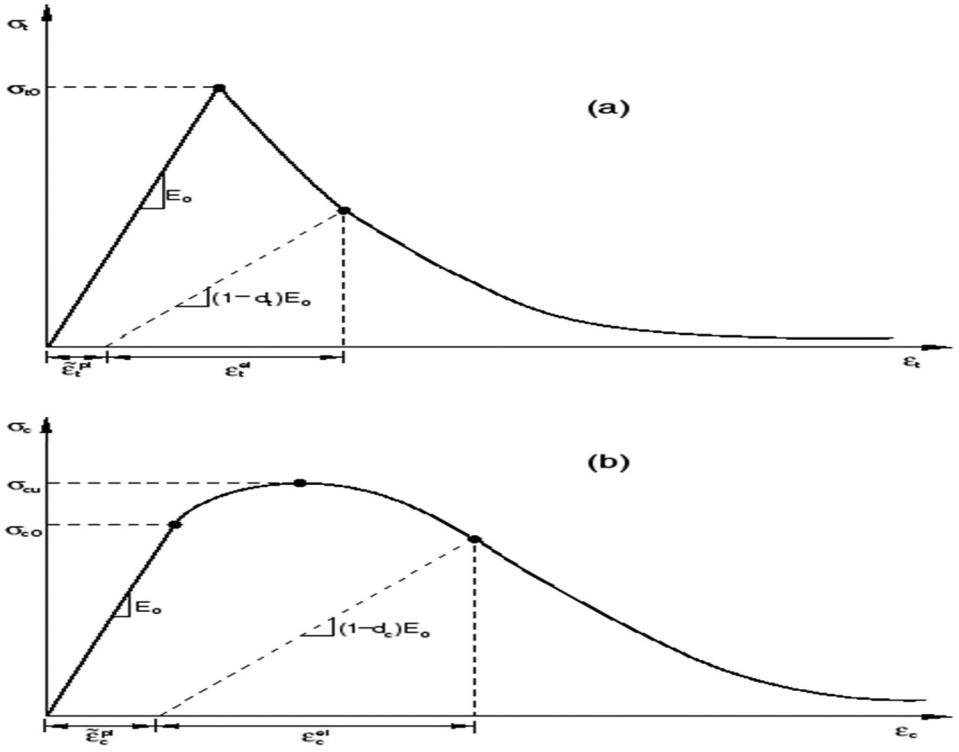

Figure 22: Stress–strain curve for (a) tension and (b) compression zone in concrete.

8 Conclusion

1. The presence of RPC caused a significant increase in the ultimate strength of the deep beams. The ultimate strength of deep beams with (RPCDB1P-4NSM and RPCDB1P-8NSM) in the present study increased by approximately (21, 25)%, respectively, of the ultimate strength of deep beams (CDB1PC20) without RPC.
2. The presence of RPC caused a significant increase in the first shear crack capacity of the deep beams. The deep beams with RPC increased by approximately (133, 150)% respectively of the ultimate strength of deep beams (CDB1PC20) without RPC.
3. Through this study, we can observe that the value of the drilling core compressive (f'_{dc}) applied based on ASTM C42/C42M-18a [28] has given a real and very different value compared with the two values of (f'_{c},) and (f'_{cu}) based on ASTM C39 [28] for the (CDB1PC20) specimen, where f'_{dc} differs with (f'_{c}, f'_{cu}) by (30, 55%), respectively, and for the (RPCDB1P-4NSM) specimen, where f'_{dc} differs from (f'_{c}, f'_{cu}) by (12, 20%), respectively.
4. The RPC of the deep beam specimen increased the strength of the specimens in all loading steps and consequently increased the deflection at the corresponding loads. The deflection of (RPCDB1P-4NSM and RPCDB1P-8NSM) was increased by about (47, 27)% at the maximum load compared to e specimen (CDB1PC20).
5. From this study, the beams (RPCDB1P-4NSM and RPCDB1P-8NSM) delayed the appearance of the first shear crack by (133, 150)%, respectively, with respect to the load compared with the beam (CDB1PC20) due to the higher shear capacity of specimens (RPCDB1P-4NSM and RPCDB1P-8NSM). Moreover, the beams (RPCDB1P-4NSM and RPCDB1P-8NSM) reduced the first shear crack width by (9, 33.25)%, respectively, compared with the beam (CDB1PC20) at 65% of the ultimate shear load.
6. From the drilled core test based on ASTM C42/C42M-18a [28] applied on beams (RPCDB1P-4NSM and CDB1PC20) real has observed that the stress results of (RPCDB1P-4NSM) have increased by (118%) at the maximum stress compared with (CDB1PC20). On the other hand, the strain results of (CDB1PC20) have increased by (22.5%) at the maximum stress compared with (RPCDB1P-4NSM).
7. From the split-cylinder test based on ASTM C496 [27], the stress–strain results, the increase in tensile stress for (RPCDB1P-4NSM) specimen at maximum stress compared with (CDB1PC20) specimen is (10%), while the increase in tensile strain for (RPCDB1P-4NSM) specimen at maximum stress is (29%).

Acknowledgments: The authors wish to thank the Fourth Dimension Contracting Company for their support, guidance, and expertise that greatly assisted the research, especially in preparing the research materials and laboratory.

Conflict of interest: The authors declare that they have no conflict of interest.

Data availability statement: Most datasets generated and analyzed in this study are comprised in this submitted manuscript. The other datasets are available on reasonable request from the corresponding author with the attached information.

References

[1] Khalifa A, Tumialan G, Nanni A, Belarbi A. Shear strengthening of continuous RC beams using externally bonded CFRP sheets. American Concrete Institute, Proc., 4th International Symposium on FRP for Reinforcement of Concrete Structures (FRPRCS4), Baltimore, MD. 1999, November. p. 995–1008.

[2] Katsumata H, Kimura K, Murahashi H. Experience of FRP strengthening for Japanese historical structures. FRP Composites in Civil Engineering. Proceedings of the International Conference on FRP Composites in Civil Engineering. Hong Kong Institution of Engineers, Hong Kong Institution of Steel Construction. Vol 2; 2001.

[3] Grace NF, Sayed GA. Construction and evaluation of full-scale CFRP prestressed concrete DT-girder. In Fibre-Reinforced Polymer Reinforcement for Concrete Structures: Vol. 2, pp. 1281–90).

[4] Rostasy FS, Neubauer U, Nothnagel R. Strengthening of historic cast iron girder with bonded CFRP plates. In: R. Seracino, editor. FRP Composites in Civil Engineering-CICE. 2004; p. 725–31.

[5] Al-Mahmoud F, Castel A, Minh TQ, François R. Reinforced concrete beams strengthened with NSM CFRP rods in shear. Adv Struct Eng. 2015;18(10):1563–74. doi: 10.1260/1369-4332.18.10.1563.

[6] Hatem M, Samad AAA, Mohamad N, Inn GW, Abdulqader S. A Review on NSM-CFRP technique using in Shear Strengthening of RC Deep Beams. Indian J Sci Technol. 2019;12(36):1–17. doi: 10.17485/ijst/2019/v12i36/147909.

[7] Saadah M, Ashteyat A, Murad Y. Shear strengthening of RC beams using side near surface mounted CFRP ropes and strips. Structures. 2021;32:380–90. doi: 10.1016/j.istruc.2021.03.038.

[8] Meier U, Deuring M, Meier H, Schwegler G. Strengthening of Structures with CFRP Laminates: Research and Applications in Switzerland. In: Neale KW, Labossière P, editors. Proceedings of the First International Conference on Advanced Composite Materials in Bridges and Structures. Sherbrooke, QC, Canada: CSCE Publication; 1992 Oct. p. 243–51.

[9] Steiner W. Strengthening of structures with CFRP strips. In: ACMBS II, MM El-Badry, editors. Second International Conference on Advanced Composite Materials in Bridges and Structures, Montréal, QC, Canada; 11–14 Aug. 1996. p. 407–17.

[10] Nanni A, Bakis CE, Boothby TE. Externally bonded FRP composites for repair of RC structures. Proceedings of the Third International Conference on Non-Metallic FRP Reinforcement for Concrete Structures, Japan. Vol. 2; 1997. p. 187–94.
[11] Matthys S, Taerwe L, Janssens J. Repair and strengthening of reptile building of the antwerp zoo. Proceedings of 1st International Conference on Innovative Materials and Technologies for Construction and Restoration, Lecca, Italy; June 6–9. Vol. 2; 2004. p. 653–63.
[12] Blasi C, Coisson E, Ferretti D. The use of carbon fibers in restoring the stables of the medici villa of Poggio a Caiano-Florence. Proceedings of First International Conference on Innovative Materials and Technologies for Construction and Restoration, Lecca, Italy. Vol. 2; 2004. p. 643–52.
[13] Labossière P, Neale KW, Martel S. Strengthening with composite materials: practical applications in quebec. In: Meier U, Betti R, editors. Proceedings of the U.S.-Europe Workshop on Recent Advances in Bridge Engineering: Advanced Rehabilitation, Durable Materials, Nondestructive Evaluation, and Management, Dubendorf and Zurich. Vol. 11; July 14–15, 1997. p. 89–96.
[14] Hazen JR, Bassett S, McDoneel VP, Dawson D, Morals L, Reque K, et al. Composites for Infrastructures: A Guide for Engineers. Wheat Ridge, CO: Ray Publishing; 1998. p. 64–5.
[15] Ichimasu H, Maruyama M, Watanabe H, Hirose T. RC slabs strengthened by bonded carbon FRP Plates Part 2—application. In: A Nanni, CW Dolan, editors. International Symposium on Fiber-Reinforced-Polymer Reinforcement for Concrete Structures. SP-138. Farmington Hills, MI: American Concrete Institute. 1993; p. 957–70.
[16] Katsumata H, Kimura K, Murahashi H. Experience of FRP strengthening for Japanese historical structures. Proceedings International Conference FRP Composites in Civil Engineering. Vol. 2. New York: Elsevier Science; 2001. p. 1001–8.
[17] Al-Mahmoud F, Castel A, François R, Tourneur C. Strengthening of RC members with near-surface mounted CFRP rods. Composite Struct. 2009;91(2):138–47.
[18] Iraqi Specification, No.5/1984. Portland Cement. 1984.
[19] Richard P, Cheyrezy M. Composition of reactive powder concretes. Cem Concr Res. 1995;25(7):1501–11.
[20] ACI Committee 243R. Guide for the use of silica fume in concrete. USA: American Concrete Institute; 1996.
[21] ASTM. Standard specification for silica fume used in cementitious mixtures. ASTM C1240-15. West Conshohocken, PA: ASTM; 2015.
[22] Standard ASTM. C494/C494M, Standard specification for chemical admixtures for concrete. West Conshohocken, PA, 29: ASTM International; 2015.
[23] ASTM. Standard specification for steel fibers for fiber-reinforced concrete. ASTM A820/A820M–11. West Conshohocken, PA: ASTM; 2011.
[24] Mezher TM, Breesem KM, Hassen DR, Jaafar AA. Stress-strain behaviour and flexural strength of silica fume polymer-modified concrete. In IOP Conference Series: Materials Science and Engineering. Vol. 881, Issue 1. IOP Publishing; 2020 July. p. 012167.
[25] ASTM S. Standard specification for deformed and plain carbon-steel bars for concrete reinforcement. ASTM A615/A615M-09b; 2009.
[26] ASTM. Standard test method for compressive strength of cylindrical concrete specimens. ASTM C39/C39M-18. West Conshohocken, PA: ASTM; 2018.
[27] ASTM C496/C496M-04. Standard test method for splitting tensile strength of cylindrical concrete specimens. Vol. 04.02; 2004. p. 5.
[28] ASTM. Standard test method for obtaining and testing drilled cores and sawed beams of concrete. ASTM C42/C42M-18a. West Conshohocken, PA: ASTM; 2018.
[29] ASTM. Standard test method for static modulus of elasticity and poisson's ratio of concrete in compression. ASTM C469-02. West Conshohocken, PA: ASTM; 2002.
[30] ACI Committee 318. Build code requir struct concr commentary. Reported by ACI Committee 318M 2014; 2014.
[31] ACI Committee-363. State of the art report on high strength concrete (ACI 363R-92). Detroit: American Concrete Institute; 1997.